Systematic characterization of THz dielectric properties of multi-component glasses using the unified oscillator model

Wada, Osamu
Ramachari, Doddoji
Yang, Chan-Shan
Uchino, Takashi
Pan, Ci-Ling

Research Article | Vol. 11, No. 3 / 1 March 2021 / Optical Materials Express 858
Optical Materials EXPRESS

Systematic characterization of THz dielectric properties of multi-component glasses using the unified oscillator model

OSAMU WADA,[1,2,8] DODDOJI RAMACHARI,[3,4] CHAN-SHAN YANG,[5,6] TAKASHI UCHINO,[7] AND CI-LING PAN[1,9]

[1]Department of Physics, National Tsing Hua University, Hsinchu 30013, Taiwan
[2]Office for Academic and Industrial Innovation, Kobe University, Kobe 657-8501, Japan
[3]Institute of Research and Development, Duy Tan University, Da Nang 550000, Vietnam
[4]Faculty of Natural Sciences, Duy Tan University, Da Nang 550000, Vietnam
[5]Institute and Undergraduate Program of Electro-Optical Engineering, National Taiwan Normal University, Taipei 11677, Taiwan
[6]Micro/Nano Device Inspection and Research Center, National Taiwan Normal University, Taipei 106, Taiwan
[7]Graduate School of Science, Kobe University, Kobe 657-8501, Japan
[8]fwga3962@nifty.com
[9]clpan@phys.nthu.edu.tw

Abstract: A terahertz (THz) dielectric property characterization method based on a unified single oscillator model has been developed and applied to a variety of multi-component silicate oxide glasses. The experimental values of dielectric constant determined by THz time-domain spectroscopy (TDS) in the sub-THz region have been confirmed to agree well with the values calculated by the single oscillator model which incorporates the local field effects and the material's ionicity. This has provided a unified formulation that enables systematic determination of the key physical parameters solely from the high-frequency (optical) and low-frequency (sub-THz) dielectric constants and characteristic resonance frequency in the (sub-)THz region. The low-frequency dielectric constant has been demonstrated to be fully determined by a single parameter of the microscopic total susceptibility. Also, the polarization ionicity, which is defined by the ionic fraction in the microscopic total susceptibility, has been found to be a good indicator to represent the ionic nature of the material. Through this analysis, an increasing trend of the effective ionic charge has been found in high-dielectric constant glasses such as oxyfluorosilicate glasses, and the physical mechanism of their dielectric constant enhancement has been discussed. The present method is expected to be applied to design and characterize dielectric properties of a wide range of multi-component glasses and other isotropic, insulating materials.

1. Introduction

Glass is one of the indispensable materials in broad applications in the terahertz (THz) region, which include a variety of systems for spectroscopy, communications, sensing and imaging functioning in the frequency range of sub-THz to tens-THz [1–4]. Particularly, glasses having high-refractive index and low-loss properties are prerequisite for forming basic passive components such as lenses and waveguides [5] as well as active components based on high optical nonlinearity [6]. A variety of silicate oxide glasses and chalcogenide glasses, which have high chemical/mechanical stability, transparency, refractive index and plausibly high optical nonlinearity, have been developed for the application in the frequency range from visible to infrared and THz regions [7,8]. Dielectric properties in the THz and sub-THz frequency ranges (THz range, in short) have been carried out by using far-infrared absorption measurement and THz-time domain spectroscopy (THz-TDS) [9–12]. Recently THz-TDS technique has been applied to characterize

#417771 https://doi.org/10.1364/OME.417771
Journal © 2021 Received 17 Dec 2020; revised 12 Feb 2021; accepted 12 Feb 2021; published 22 Feb 2021

Optical Materials EXPRESS

a variety of glass materials including silicate oxides [13–16] and chalcogenides [17–19]. Naftaly has reported a study of THz refractive index and absorption properties of a series of commercial silicate oxide glasses [15]. Ravagli has carried out a study on sub-THz refractive index and absorption coefficient in a selection of chalcogenide and La:chalcogenide glasses [17]. We have reported the fabrication and sub-THz characterization of oxyfluorosilicate (OFS) glasses as a new group of multi-component silicate oxide glasses [20], in which fluorides (ZnF_2, PbF_2 and LiF), rare-earth ions (Nd^{3+}), alkali ions (K^+ and Na^+) and intermediate network former Nb_2O_5 are incorporated. An OFS glass containing 20 mol % of Nb_2O_5 (i.e. ZNbKLSNd glass) has achieved the simultaneous realization of the highest refractive index (2.9-3.7) and lowest absorption loss (6-9 cm^{-1}) among silicate oxide glasses in sub-THz frequency region [20].

For designing and characterizing glass material's physical and chemical properties in the THz frequency region, it is essential to understand the THz dielectric properties on the basis of a common physical model. In this view, we have recently reported a study on the dielectric properties of OFS glasses using THz-TDS [21] and optical reflectivity measurements, and results have been compared with other multi-component silicate oxide glasses [15] and chalcogenide glasses [17]. The static refractive indices in sub-THz and optical frequency regions have been analyzed using the Clausius-Mossotti equation (Lorentz-Lorentz equation) [22,23] for determining the electronic and ionic polarizabilities [15]. The ionic to electronic polarizability ratio has been used to evaluate the ionic contribution to the sub-THz dielectric constant [21]. The dynamic property of sub-THz dielectric constant has been analyzed by using the damped harmonic oscillator model (Lorentz model [1, 3, 9, 22, 23]), and its viability has been confirmed in glasses [21]. The usefulness of THz characterization has thus been proven in various glass materials. However, most of the previous optical studies on the physical/chemical properties of multi-component silicate oxide glasses have been carried out only in the visible to infrared frequency region, and the collected data have shown considerable scattering among different glasses [24].

For systematically and fully understanding fundamental nature of various silicate oxide glasses, a more precise, unified THz dielectric model is required. More specifically, the local field correction and ionicity effects should be taken explicitly in the dielectric property analysis. The local field effect gives a significant addition to the microscopic field at an atom site, therefore it should be considered in precise evaluation of the dielectric constant. Since the effect has not been considered in the simplified single oscillator model as used in [21], it is more relevant to take the effect explicitly into the oscillator model in THz region. In order to closely investigate the ionicity or the ionic/electronic contributions to dielectric properties, the dielectric dispersion in (sub)THz region, which reveals the dynamics of ionic vibration, is essential. The THz dielectric dispersion properties have been studied so far by using the Lorentz model for insulating materials [1, 3, 9, 21] and the Drude [22,23] and Drude-Smith [25] models for conducting materials, but very few attempts have been made to fully include the ionic/electronic contributions to the THz dielectric dispersion properties in glasses. For analyzing the static dielectric constant properties, the Clausius-Mossotti relation can be adequately used, since it has been derived from the local field effect consideration. On the other hand, we need an appropriate method to analyze the dynamic dielectric constant characteristics in the THz region.

The purpose of the present study is to build up a unified characterization method on the basis of single oscillator model to fully understand the THz and optical dielectric properties in multi-component glasses. This is achieved by the application of single oscillator based dielectric function which incorporate the local field correction and material's ionicity effects. It is also shown that only a couple of parameters obtained from THz-TDS and optical reflectance measurements (namely, the THz- and optical-dielectric constants and the (sub)THz characteristic resonance frequency) can provide basic parameters (namely, the total microscopic susceptibility and the polarization iconicity which will be detailed later) for fully analyzing dielectric properties

Optical Materials EXPRESS

of materials. In this study, although we focus on experimental results of silicate oxide multi-component glasses including OFS glasses and several commercial glasses by using previous publications [15, 20, 21], the characterization method itself should be applicable to a wide range of non-crystalline, non-conducting materials.

In the rest of the present paper, we first describe glass samples and data acquisition in Section 2. Section 3 summarizes the relationship between the static THz and optical dielectric constants for different glasses. In Section 4, we describe the single oscillator based dielectric model including the local field effects to analyze the THz dielectric constant. New parameters indicating the polarization ionicity are introduced and used for fully interpreting the dielectric constant properties of different families of glass. In Section 5, we analyze the frequency-amplitude correlations in ionic oscillator characteristics and discuss possible physical/chemical origin of dielectric constant enhancement. Section 6 summarizes the paper.

2. Glass samples and data acquisition

The multi-component silicate oxide glass samples considered here include our own OFS glasses and several other commercial glasses. Dielectric property data were acquired either by our experiments or from literature. The OFS glass samples used involve two glass groups [20]; one is ZNbKLSNdx: (20-x)ZnF_2 + 20Nb_2O_5 + 20K_2CO_3 + 10LiF + 30SiO_2 + $x$$Nd_2O_3$, and the other is PbNKLSNdx: (20-x)PbF_2 + 5Na_2O + 20K_2CO_3 +10LiF + 45SiO_2 + $x$$Nd_2O_3$, where x = 1, 5 and 10 mol%. OFS glasses were prepared by the melt-quenching technique as reported in our report [20]. The THz optical constants of OFS glasses were determined by using a photoconductive-antenna-based transmission type THz-TDS system [25]. The optical transmission and reflectivity were measured by using the conventional Fourier transform infrared (FTIR) spectroscopy system in the visible to near-infrared range, and the optical refractive indices have been determined using the standard methods [21]. Compositions and basic physical parameters of glasses are summarized in Table 1.

Table 1. Compositions and basic physical parameters of a variety of silicate oxide glasses.

Glass	Composition		M (g/mol)	ρ (g/cm^3)	V_m (cm^3/mol)	Ref
ZNbKLSNdx	(20-x)ZnF_2+20Nb_2O_5+20K_2CO_3+ 10LiF+30SiO_2 +$x$$Nd_2O_3$	x=1	124	3.65	34.0	[20,21]
		x=5	133	3.66	36.3	
		x=10	145	3.54	41.0	
PbNKLSNdx	(20-x)PbF_2+5Na_2O+20K_2CO_3+ 10LiF+45SiO_2+ $x$$Nd_2O_3$	x=1	110	3.72	29.7	[20,21]
		x=5	114	3.78	30.2	
		x=10	119	3.62	32.8	
Silica	SiO_2		60	2.20	27.3	[15,21]
Pyrex	80.6SiO_2+12.6B_2O_3+4.2Na_2O+2.2Al_2O_3+ 0.04Fe_2O_3+0.1CaO+0.05MgO+0.1Cl		62	2.23	27.8	[15,21]
BK7	68.9SiO_2+10.1B_2O_3+8.8Na_2O+8.4K_2O+ 2.8BaO+1.0As_2O_3		65	2.51	26	[15,21]
SK10	30.6SiO_2+11.7B_2O_3+5.0Al_2O_3+0.1Na_2O+ 48.2BaO+2.0ZnO+0.7PbO+0.8Sb_2O_3+ 0.9As_2O_3		112	3.64	30.8	[15,21]
SF10	35.3SiO_2+2.0Na_2O+2.5K_2O+55.7PbO+ 4.0TiO_2+0.5As_2O_3		153	4.28	35.8	[15,21]
SF6	27.7SiO_2+0.5Na_2O+1.0K_2O+70.5PbO+ 0.3As_2O_3		177	5.18	34.2	[15,21]

Optical Materials EXPRESS

3. Static dielectric constants in the THz and optical frequency regions

As discussed in our previous study [20,21], the static dielectric constant characteristics of silicate oxide are analyzed by using the Clausius-Mossotti equation (Lorentz-Lorentz equation) [15, 22, 23]. The dielectric constant $\varepsilon_{\mathrm{opt}}$ in the optical frequency range is determined by the polarizability of electrons associated with constituent molecules in the glass. On the other hand, the dielectric constant $\varepsilon_{\mathrm{THz}}$ in the sub-THz frequency range is determined by the total polarizability including contributions not only of fast response electrons (α) but also of slow response ions (α_{i}) in the glass. Thus the dielectric constants, $\varepsilon_{\mathrm{opt}}$ and $\varepsilon_{\mathrm{THz}}$, are related to the molar electronic polarizability, α, molar ionic polarizability, α_{i}, and molar total polarizability, $\alpha_{\mathrm{tot}} = \alpha + \alpha_{\mathrm{i}}$, as shown in the following relations (in SI unit):

$$\frac{\varepsilon_{opt} - 1}{\varepsilon_{opt} + 2} V_m = \frac{1}{3\varepsilon_0} N_A \alpha = R_m^e, \tag{1}$$

$$\frac{\varepsilon_{THz} - 1}{\varepsilon_{THz} + 2} V_m = \frac{1}{3\varepsilon_0} N_A (\alpha + \alpha_i) = R_m^{tot} = R_m^e (1 + a), \tag{2}$$

where V_{m} is the molar volume defined by M/ρ using the molecular weight M and density ρ, N_{A} is the Avogadro number (6.023×10^{23} mol^{-1}), R_m^e is the molar electronic refraction, R_m^{tot} is the molar total refraction including both electronic and ionic contributions, and a is defined as the ionic to electronic polarizability ratio: $\alpha_{\mathrm{i}}/\alpha$. Taking account of the negligibly small extinction coefficient ($k=\alpha_{\mathrm{abs}}c/2\omega$, a_{abs}: absorption coefficient, c: speed of light, ω: light angular frequency) in comparison with the refractive index in the sub-THz region in those glasses [21], the dielectric constant $\varepsilon_{\mathrm{THz}}$ is obtained from $\varepsilon_{\mathrm{THz}}=n_{\mathrm{THz}}{}^2$ using the refractive index values determined at the low frequency (0.2 THz) in the THz-TDS measurements. Similarly the optical dielectric constant $\varepsilon_{\mathrm{opt}}$ is obtained from $\varepsilon_{\mathrm{opt}}=n_{\mathrm{opt}}{}^2$ using the optical refractive index value determined at the wavelength of 1500 nm in the reflection measurement.

All the sub-THz range data have been collected from our experiments [20,21] and from literature [15], and basic parameters are summarized in Table 2. Figure 1(a) shows the plots of measured $\varepsilon_{\mathrm{THz}}$ as a function of $\varepsilon_{\mathrm{opt}}$ for multi-component glasses, and curves in the figure have been calculated from equations: $\varepsilon_{\mathrm{opt}}=(1+2b)/(1-b)$ and $\varepsilon_{\mathrm{THz}}=(1+2(1+a)b)/(1-(1+a)b)$, where $b=R_m^e/V_m$, which are readily derived from Eqs. (1) and (2) [21]. The dielectric constant values measured for various silicate oxide glasses follow these relationships with the parameter a determined by fitting for each glass, and the resultant a value is displayed as a function of $\varepsilon_{\mathrm{opt}}$ in

Table 2. Material, THz, and optical parameters determined for glasses used in the present analysis.

Glass	$\varepsilon_{\mathrm{THz}}$	$\varepsilon_{\mathrm{opt}}$	a	$\omega_{\mathrm{T}}{}^2$ (x10^2 THz^2)	$\omega_P{}^{*2}/w_T{}^2$	$n\alpha$	ω_P/ω_0	ω_T/ω_0	Ref
ZNbKLSN01	13.54	3.27	0.868	6.39	10.26	1.294	1.061	0.583	[21]
ZNbKLSN05	13.69	3.20	0.947	5.71	10.49	1.271	1.075	0.576	[21]
ZNbKLSN10	13.32	3.24	0.850	3.65	10.08	1.282	1.063	0.585	[21]
PbNKLSN01	8.70	2.46	1.23	2.22	6.238	0.984	1.084	0.646	[21]
PbNKLSN05	9.24	2.66	1.09	2.80	6.585	1.067	1.064	0.644	[21]
PbNKLSN10	8.76	2.34	1.38	2.66	6.421	0.927	1.112	0.635	[21]
Silica	3.84	2.13	0.808		1.710	0.822	0.799	0.841	[15]
Pyrex	4.43	2.16	0.954		2.270	0.837	0.874	0.804	[15]
BK7	6.30	2.31	1.14	5.44	3.990	0.912	1.002	0.721	[15]
SK10	8.47	2.62	1.03	2.21	5.844	1.053	1.042	0.665	[15]
SF10	10.30	2.99	0.896	1.85	7.311	1.197	1.035	0.637	[15]
SF6	12.67	3.28	0.841	2.02	9.398	1.294	1.046	0.600	[15]

Optical Materials EXPRESS

Fig. 1(b). Such a relationship implies the usefulness of this parameter for characterizing different glass properties, but its behavior is not monotonous for ε_{opt} as shown in Fig. 1(b). Although we have discussed in our previous paper [21] possible interpretations in conjunction with the material's ionicity/covalency, no rigid conclusion has been reached. We will come back to this issue at the end of Sec. 4.2.

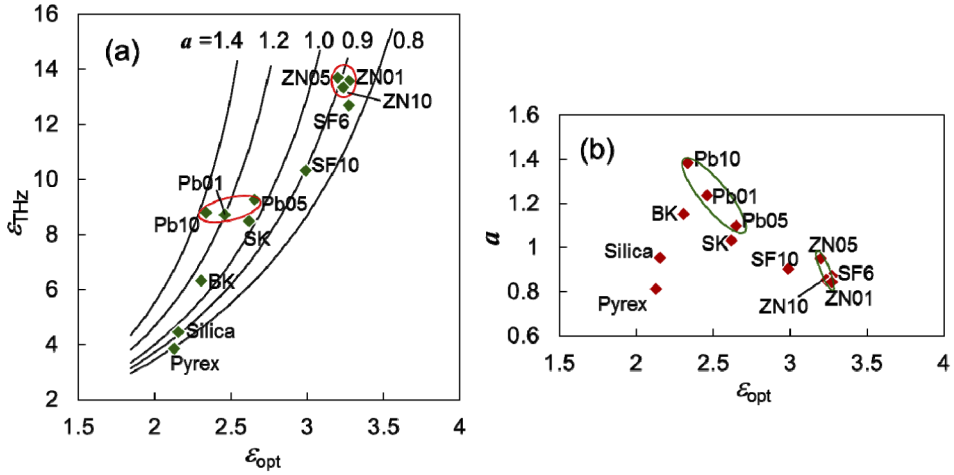

Fig. 1. Relationships of (a)THz dielectric constant and (b) parameter a defined by the ratio of the ionic to electronic polarizabilities as functions of optical dielectric constant for different silicate oxide glasses.

4. Dielectric property analysis based on single oscillator model

4.1. Single oscillator based formalism for dielectric property analysis

In our previous study [21], a simplified form of single oscillator model has been confirmed to be applicable as a unified model to describe the THz dielectric constant characteristics for all the examined silicate oxide glasses. However, the analysis method adopted there only assumes the diatomic chain vibration and does not represent explicitly the local field effect. To properly discuss the behavior of electromagnetic waves induced by ionic vibration, the application of phonon polariton formalism with the inclusion of the local field effect is useful [22,23,26,27]. In the following, we summarize the basic dielectric function and derive further some useful relations for characterizing dielectric properties by referring to Gresse's approach [28].

We assume a simple diatomic chain based single oscillator model for describing (analogously) the "lattice" (ion) vibration to determine the dielectric functions of glass materials. An equation of motion for the relative displacement of the cation-anion pair $\mathbf{u}$ is given in the following form:

$$\mu\ddot{\mathbf{u}} + \mu\gamma\dot{\mathbf{u}} + D\mathbf{u} = q^{*}\mathbf{E}_{loc}, \tag{3}$$

where μ is the reduced mass of ions defined by $1/\mu = 1/m_{+} + 1/m_{-}$, where m_{+} and m_{-} are the masses of anion and cation, γ is the damping factor for displacement, D is the force constant of the ionic pair, q^{*} is the effective charge of ion. $\boldsymbol{E}_{loc}$ is the local electric field which involves the microscopic Lorenz field applied to an atom and is correlated with the macroscopic applied field $\boldsymbol{E}_{a}$ and polarization $\mathbf{P}$ by:

$$\mathbf{E}_{loc} = \mathbf{E}_{a} + \frac{1}{3}\cdot\frac{\mathbf{P}}{\varepsilon_0} = \left(\frac{1}{\chi} + \frac{1}{3}\right)\frac{\mathbf{P}}{\varepsilon_0}, \tag{4}$$

where a macroscopic relation of the applied field $\mathbf{E}_{a}$ with the polarization, $\mathbf{P} = \varepsilon_0\chi\mathbf{E}_{a}$, has been used. Here, ε_0 and χ are the vacuum dielectric constant and macroscopic electric susceptibility

Optical Materials EXPRESS

of the material. The total polarization **P** consists of the lattice strain (**u**) induced dipole moment originated from the relative ion core displacement ($\mathbf{P}_{PH}$) and the polarization due to the valence electron displacement with respect to ion core in the local field ($\mathbf{P}_{VE}$) as is expressed by:

$$\mathbf{P} = \mathbf{P}_{PH} + \mathbf{P}_{VE} = nq^*\mathbf{u} + n\varepsilon_0\alpha\mathbf{E}_{loc}, \tag{5}$$

where n is the number of atoms in unit molecule ($n = N_A/V_m$) and α is the electronic polarizability of valence electrons with respect to steady ion core (without lattice strain). The effect of valence electron displacement induced by the lattice strain is incorporated in the effective charge q^* of ion pair. Under the application of harmonic electric field ($\mathbf{E}_a \propto \exp(-i\omega t)$), Eq. (3) is written in the following form:

$$(\omega^2 + i\omega\gamma - {\omega_0}^2)\mathbf{u} + \frac{q^*}{\mu}\mathbf{E}_{loc} = 0, \tag{6}$$

where ω_0 is defined as ${\omega_0}^2 = \frac{D}{\mu}$ by using the force constant D, and ω_0 indicates the intrinsic resonance frequency for the undamped vibration of diatomic chain under zero electric field: $\ddot{\mathbf{u}} + {\omega_0}^2\mathbf{u} = 0$.

Equations (4)–(6) form a set of homogeneous equations for **u**, **P** and $\mathbf{E}_{loc}$ and they comprise the basic phonon polariton formulation (Huang-Szigetti equation). By solving the secular equation for the macroscopic susceptibility χ, the following relation is obtained:

$$\chi = \frac{3(n\alpha + \chi_0)}{3 - (n\alpha + \chi_0)}. \tag{7}$$

Here, $n\alpha$ and χ_0 indicate the microscopic electronic and ionic susceptibilities. The microscopic ionic susceptibility, χ_0, is induced by the ionic vibration, in which effects of valence electron polarization ($n\varepsilon_0\alpha\mathbf{E}_{loc}$) and the induced local field ($\mathbf{P}/3\varepsilon_0$) are excluded, and is expressed by:

$$\chi_0 = \frac{{\omega_p}^2}{{\omega_0}^2} \cdot \frac{{\omega_0}^2}{{\omega_0}^2 - \omega^2 - i\omega\gamma}. \tag{8}$$

where, ω_p is the ionic vibration resonance frequency which is defined by ${\omega_p}^2 = \frac{nq^{*2}}{\varepsilon_0\mu}$.

It is readily proved that the macroscopic susceptibility as shown by Eq. (7) can be renormalized into a form similar to Eq. (8):

$$\chi = \chi_\infty + \frac{{\omega_p}^{*2}}{{\omega_T}^2} \cdot \frac{{\omega_T}^2}{{\omega_T}^2 - \omega^2 - i\omega\gamma}, \tag{9}$$

where χ_∞ is the value of χ at the high frequency limit ($\omega \to \infty$), and is related to $n\alpha$ and ε_∞ through $\varepsilon = 1 + c$ as:

$$\chi_\infty = \varepsilon_\infty - 1 = \frac{3n\alpha}{3 - n\alpha}. \tag{10}$$

As shown by Eq. (9), the macroscopic susceptibility comprises the contributions of the valence electrons $\chi_{VE} = \chi_\infty$ and the contribution of the lattice vibration (χ_{PH}) as given by the second term. In Eq. (9), the renormalized characteristic frequency ω_T is defined as:

$${\omega_T}^2 = {\omega_0}^2 - \frac{1}{3 - n\alpha}{\omega_p}^2 = {\omega_0}^2 - \frac{1}{3}{\omega_p}^2\frac{\chi_\infty + 3}{3} = {\omega_0}^2 - \frac{1}{3}{\omega_p}^2\frac{\varepsilon_\infty + 2}{3}, \tag{11}$$

and the following conditions are satisfied:

$$\frac{{\omega_p}^{*2}}{{\omega_T}^2} = \chi_s - \chi_\infty = \varepsilon_s - \varepsilon_\infty, \tag{12}$$

Optical Materials EXPRESS

$$\omega_p{}^*2 = \omega_p{}^2\left(\frac{\chi_\infty + 3}{3}\right)^2 = \omega_p{}^2\left(\frac{\varepsilon_\infty + 2}{3}\right)^2 = \frac{nq^{*2}}{\varepsilon_0\mu}\left(\frac{\varepsilon_\infty + 2}{3}\right)^2, \tag{13}$$

where χ_s and ε_s are the values of χ and ε at the low frequency limit ($\omega\rightarrow 0$). Thus the dielectric function as given by Eq. (9) can be expressed also by:

$$\varepsilon = \varepsilon_\infty + (\varepsilon_s - \varepsilon_\infty)\frac{\omega_T{}^2}{\omega_T{}^2 - \omega^2 - i\omega\gamma}, \tag{14}$$

which corresponds to the simplified form of dielectric function as used previously [21].

In order to look into the contribution of the ionic vibration or lattice strain ($\propto nq^*$) and that of the valence electron displacement ($\propto n\alpha$) to determine the total polarization, it is worth to see the behavior of dielectric parameters such as the dielectric constants, ε_∞ and ε_s, and the renormalized characteristic frequency, ω_T, etc. as functions of the microscopic electronic susceptibility $n\alpha$ and the microscopic ionic susceptibility amplitude $(\omega_p/\omega_0)^2$ (Eq. (8)). For this purpose, the following equations are deduced from Eqs. (9), (11) and (12):

$$\varepsilon_\infty = \frac{3 + 2n\alpha}{3 - n\alpha}, \tag{15}$$

$$\varepsilon_s = \frac{3 + 2((n\alpha + (\omega_p/\omega_0)^2)}{3 - ((n\alpha + (\omega_p/\omega_0)^2)}, \tag{16}$$

$$\frac{\omega_T}{\omega_0} = \left(1 - \frac{1}{3 - n\alpha}\left(\frac{\omega_p}{\omega_0}\right)^2\right)^{1/2}. \tag{17}$$

It would be noteworthy that we can also deduce from Eqs. (9)–(15) very simple and convenient relations to determine $n\alpha$, ω_p/ω_0 and other parameters by using only the steady state values of dielectric constants, ε_s and ε_∞, as shown in the following:

$$n\alpha = \frac{3(\varepsilon_\infty - 1)}{\varepsilon_\infty + 2}, \tag{18a}$$

$$\frac{\omega_p}{\omega_0} = \left(\frac{9(\varepsilon_s - \varepsilon_\infty)}{(\varepsilon_s + 2)(\varepsilon_\infty + 2)}\right)^{1/2}, \tag{18b}$$

$$\frac{\omega_T}{\omega_0} = \left(\frac{\varepsilon_\infty + 2}{\varepsilon_s + 2}\right)^{1/2}. \tag{18c}$$

Considering $\varepsilon_\infty = \varepsilon_{opt}$ and $\varepsilon_s = \varepsilon_{THz}$ and Eqs. (1) and (2), also the ionic to electronic polarizability ratio a is expressed by:

$$a = \frac{\alpha_i}{\alpha} = \frac{3(\varepsilon_s - \varepsilon_\infty)}{(\varepsilon_s + 2)(\varepsilon_\infty - 1)}. \tag{18d}$$

Although relations of Eqs. (18a–c) have been described in literature [26,27], their practical significance has not been recognized fully. The most important advantage of these equations is in that only obtaining the data of ε_s, ω_T (from THz-TDS) and ε_∞ (from optical measurement, e.g. reflectance) is sufficient for determining all basic physical parameters necessary for material assessment. This can provide a simple method of comparing low (e.g. sub-THz) frequency dielectric properties even among different glasses as far as the single oscillator model is relevant.

Optical Materials EXPRESS

4.2. Comparison between theory and experiment

In this section we analyze the measured dielectric properties of different glasses by using the relations described above. The values of the renormalized characteristic frequency ω_T and amplitude factor ${\omega_p}^{*2}$ of the oscillator are determined from the measured frequency dependence of dielectric constant in sub-THz region using the method same as used in our previous study [21]. The renormalized characteristic frequency ω_T corresponds to the characteristic resonance wavelength λ_0 as used in our previous study [21] (also refer to Sec.5) through $\omega_T = 2\pi c/\lambda_0$. Using this ${\omega_p}^{*2}$, ${\omega_p}^{*2}/{\omega_T}^2 = \varepsilon_s - \varepsilon_\infty$ (Eq. (12)) is calculated. Then the value of ω_0 as well as ω_p/ω_0 and ω_T/ω_0 are determined by using Eqs. (11)–(13) for each glass. Table 2 summarizes the obtained parameters including $n\alpha$ calculated from Eq. (18a).

Figure 2 shows three-dimensional maps for the evaluated results of (a) ε_s, (c) ω_T/ω_0, (e) ε_∞, and (f) a parameter on the planes of $n\alpha$ and ω_p/ω_0. Plots in (b) and (d) show the experimental data of (b) ε_s and (d) ω_T/ω_0 evaluated by using measured values of ε_∞ and ε_s. As is shown in (e) and also in Eq. (15), ε_∞ is independent from the ionic contribution and solely determined by the polarization due to valence electrons. On the other hand ε_s depends on both the electrons and ions and increases steeply as their contributions increase as is shown in (a). The contour as delineated for $n\alpha < 3$ and $\omega_p/\omega_0 < 3^{1/2}$ on the base plane shows the limit of existence of ε_s where the catastrophic collapse of glass phase occurs and the dielectric constant diverges to infinity. In figure (b), experimental data of ε_s are plotted for different silicate oxide glasses and also for two La:chalcogenide glasses [17,21] for reference. As for OFS glasses, only data for x=5 are shown for avoiding complexity of the figure. The comparison between figures (a) and (b) indicates a good correspondence between the experimental and calculated results for all glasses. Since chalcogenide glasses are known to be highly covalent in comparison with silicate oxide glasses, they appear at locations with higher $n\alpha$ and lower ω_p/ω_0 than for silicate oxide glasses.

In Fig. 2(c) and (d), calculated and measured values of ω_T/ω_0 are plotted (for OFS glasses, x=5 only) with a viewing angle changed for easier inspection of the overall trend. It is clearly seen that as increasing the electronic and ionic contributions, the characteristic frequency exhibits a softening towards the catastrophic boundary where ω_T vanishes and the dielectric constant diverges. Again the experimental data support the calculated trend. This softening behavior of ω_T/ω_0 corresponds to the increase in the dielectric constant, and can be used for characterizing the dielectric properties of materials. Figure 2(f) shows the values of a parameter estimated by Eq. (18d), which shows non-monotonous behavior in contrast with ε_∞ or ε_s.

For more precise theory-measurement comparison, the relationships of ε_s, ω_T/ω_0 and a as functions of ω_p/ω_0 using $n\alpha$ as a parameter are shown in Fig. 3, in which all measured data are also displayed. Those results suggest that the dielectric parameters in the glasses examined here are largely influenced by the ionic vibration originated polarization ($(\omega_p/\omega_0)^2$) but precise parameter values are modified by the valence electron polarization effect ($n\alpha$). This explains the reason of data scattering in the ε_s versus ε_∞ relationship as noticed in Fig. 1(a), and precise values of $n\alpha$ should be determined through curve fitting processes. The present results in Fig. 3 have confirmed the consistency between the model and experiment. It has been confirmed that values of key parameters necessary for the analysis, such as $n\alpha$, ω_p/ω_0 and ω_T/ω_0, can be determined simply from Eqs. (18a)–(18d).

We here have a look at the behavior of the a parameter. It is noticed that the envelope of a parameter drawn on the $n\alpha - \omega_p/\omega_0$ plane is warped (Fig. 2(f)) differently when compared with the envelopes of ε_∞ (Fig. 2(e)) and ε_s (Fig. 2(a)). In Fig. 1(b), a nonmonotonous (double-valued) behavior of a parameter as a function of ε_{opt} is found. Such a nonmonotonous relationship is readily understood by taking account of the difference in envelope warp for a and ε_∞: when $n\alpha$ increases, ε_∞ also increases, whereas a parameter can either increase or decrease depending on the value of ω_p/ω_0.

Optical Materials EXPRESS

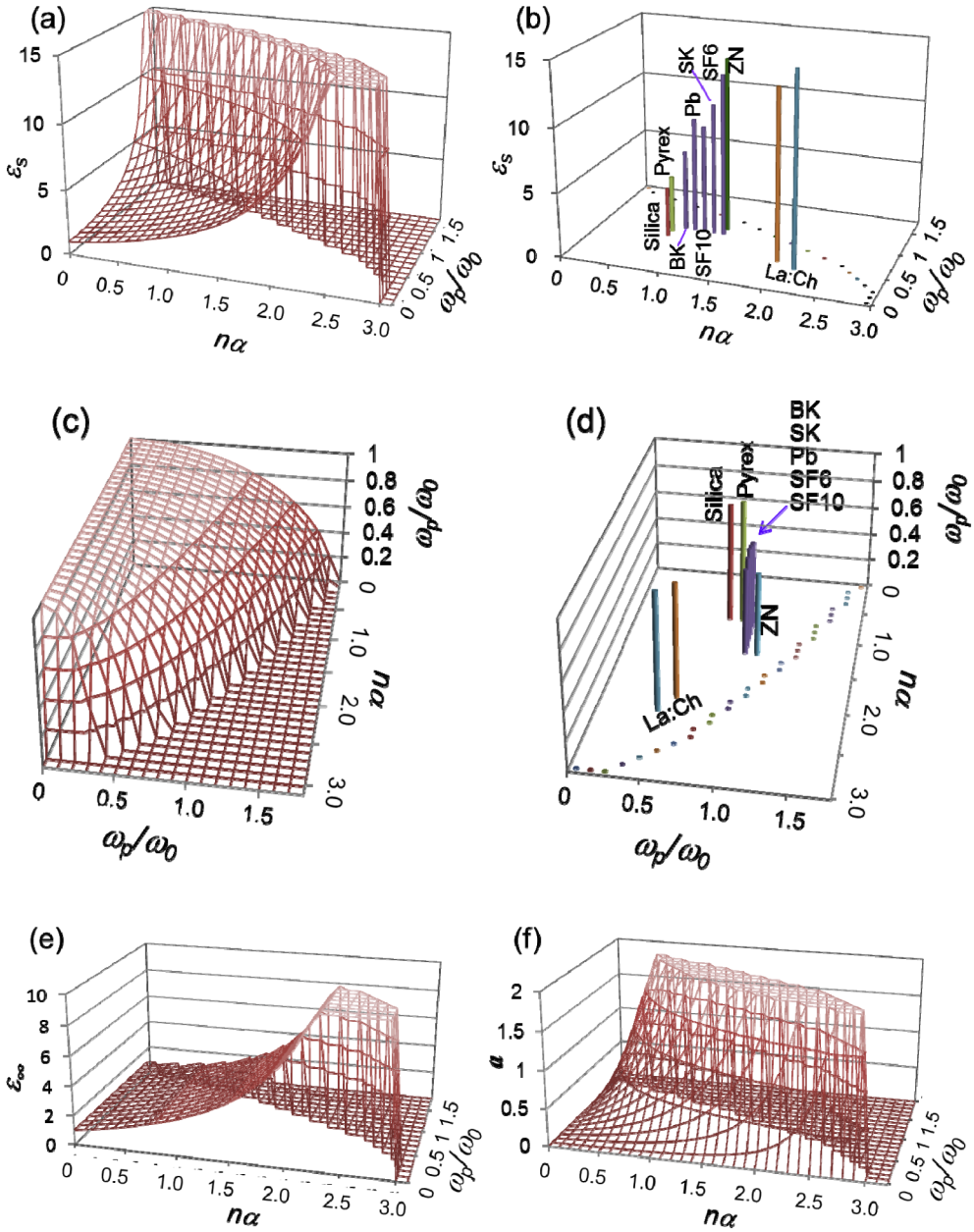

Fig. 2. A variety of the dielectric parameters (a),(b) ε_s, (c),(d) ω_T/ω_0, (e) ε_∞, and (f) a= α_i/α in the planes of $n\alpha$ and ω_p/ω_0. Plots (a), (c), (d) and (f) show the calculated results using Eqs. (10)–(13), and plots (b) and (d) show experimental data evaluated by measured values of ε_∞ and ε_s using Eqs. (15)–(18).

Optical Materials EXPRESS

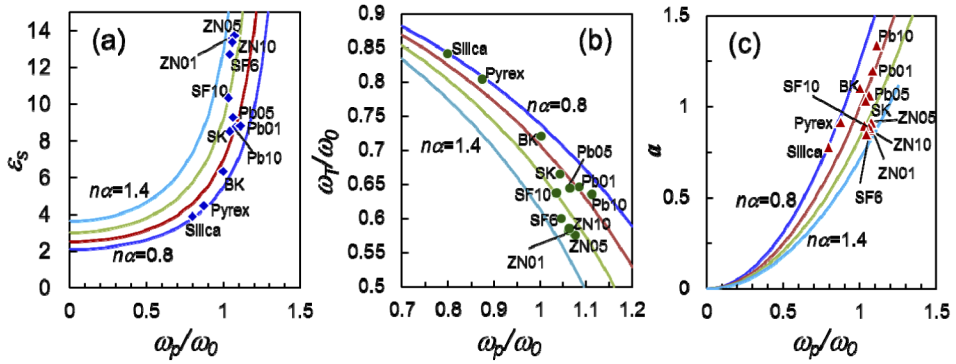

Fig. 3. Calculated curves of (a) ε_s, (b) ω_T/ω_0, and (c) $a = \alpha_i/\alpha$ as functions of ω_p/ω_0 using $n\alpha$ as a parameter. The values of $n\alpha$ is varied by 0.2 from 0.8 to 1.4, and symbols show measured data.

4.3. *Effect of the ionic contribution to the low-frequency dielectric constant*

Although two parameters $n\alpha$ and ω_p/ω_0 are necessary to precisely formulate the dielectric characteristics of silicate oxide glasses as discussed above, it would be even more convenient if a single parameter could represent the dielectric characteristics. Such a parameter can be defined at least for representing ε_s. As is known from Eq. (7), the catastrophic boundary projected on the $n\alpha$–ω_p/ω_0 plane is given by $n\alpha+(\omega_p/\omega_0)^2=3$, which is nothing but a circle on the $(n\alpha)^{1/2}$–(ω_p/ω_0) plane. Therefore ε_s has an axial symmetry on the $(n\alpha)^{1/2}$–(ω_p/ω_0) plane, and its value is uniquely determined by the total microscopic susceptibility R^2, which is defined as the sum of the microscopic electronic $(n\alpha)$ and ionic $((\omega_p/\omega_0)^2)$ susceptibilities:

$$R^2 = n\alpha + (\omega_p/\omega_0)^2 = \frac{3(\varepsilon_s - 1)}{\varepsilon_s + 2}. \tag{19a}$$

To obtain precise values of other parameters such as ω_T/ω_0 and a, however, another quantity is still required to represent the balance between the valence electron contribution $(n\alpha)$ and ionic vibration contribution $((\omega_p/\omega_0)^2)$ to R^2. Considering that these factors stand for the polarization contributions which govern the dielectric constant, we define here the polarization ionicity I_P by the following expression:

$$I_P = \frac{(\omega_p/\omega_0)^2}{R^2} = \frac{(\omega_p/\omega_0)^2}{n\alpha + (\omega_p/\omega_0)^2} = \frac{3(\varepsilon_s - \varepsilon_\infty)}{(\varepsilon_s - 1)(\varepsilon_\infty + 2)}. \tag{19b}$$

By using R and I_P, relations to determine all values of $n\alpha$, ω_p/ω_0 and other dielectric parameters can be rewritten as shown in the following:

$$n\alpha = R^2(1 - I_P), \tag{20a}$$

$$\frac{\omega_p}{\omega_0} = (R^2 \cdot I_P)^{1/2}, \tag{20b}$$

$$\varepsilon_\infty = \frac{3 + 2R^2(1 - I_P)}{3 - R^2(1 - I_P)}, \tag{20c}$$

$$\varepsilon_s = \frac{3 + 2R^2}{3 - R^2}, \tag{20d}$$

$$\frac{\omega_T}{\omega_0} = \left(\frac{3 - R^2}{3 - R^2(1 - I_P)}\right)^{1/2}, \tag{20e}$$

Optical Materials EXPRESS

$$a = I_P/(1 - I_P). \tag{20f}$$

Table 3 shows the values of R^2 and I_P obtained for all glasses examined. Figure 4 displays the dielectric parameters as functions of R^2. Symbols show data measured for all silicate oxide glasses except for silica and Pyrex; the values of ω_T/ω_0 for these two glasses have been calculated by Eq. (20) using the static dielectric constant values ε_s and ε_∞. Curves in the figure have been calculated using I_P=0.5 or a=1, which are shown as straight dotted lines in Fig. 4(b) to guide the eye. As is obvious in Fig. 4(a), ε_s shows a perfect match between the calculation and experimental data. Other two parameters, ε_∞ and ω_T/ω_0, also show reasonable matches for a constant I_P=0.5, primarily due to a fairly small variation of I_P for all glasses considered here. Thus the present way of analysis provides a systematic understanding of low-frequency dielectric constant. It is also understood from the similarity between the trends of I_P and a as shown in Fig. 4(b) as well as from Eq. (20f) that both of I_P and a represent basically the same characteristics of ionic contribution to the low-frequency dielectric constant. Therefore the polarization ionicity can be used more conveniently than the a parameter due to its monotonous behavior on the $n\alpha$ -ω_p/ω_0 plane. (also refer to Sec. 4.4)

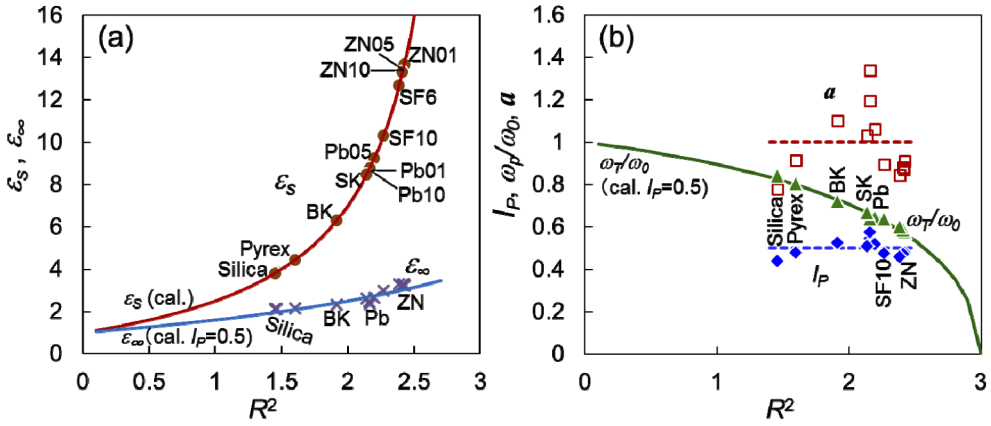

Fig. 4. Measured data of (a) ε_s and ε_∞, and (b) polarization ionicity I_P, relative characteristic frequency ω_T/ω_0 and a parameter as functions of R^2. Curves show calculated relationships. Dotted lines are guide for the eye for I_p=0.5 and a=1.

4.4. *Correlation of ionic contribution with electronegativity difference*

Effects of the ionic and covalent contributions to material properties have been studied extensively for a variety of dielectric and semiconducting materials [29–31]. Pauling [32] has empirically defined the bond ionicity I_b=1-exp(-0.25(ΔX)^2), where ΔX is the electronegativity difference of the material, and this scale is often used for discussing chemical bond energy and electronic structure of materials [33]. For oxide glass materials, the ionicity/covalency characteristics have been discussed in terms of the bandgap energy [34] and refractive index in the optical frequency region [34–36]. Although these models have provided reasonable interpretations for materials with rather simple compositions, there have been no attempts in literature to investigate low-frequency (sub-THz) dielectric constants in multi-component glasses. In contrast with previous methods, the definition of the polarization ionicity I_P as described above is definitely straightforward in regard to describe the low frequency dielectric constant. Here we examine the relationship between the present polarization ionicity I_P with Pauling's bond ionicity I_b for multi-component silicate oxide glasses. Figure 5(a) shows the plot of I_P as a function of the electronegativity difference, ΔX. To estimate ΔX, first the electronegativity difference for each

Optical Materials EXPRESS

of constituent oxides and fluorides are calculated by geometrical mean [37] using Pauling's electronegativity values [38], and the overall ΔX is obtained as the compositional average of these values [30] as summarized in Table 3. A line in Fig. 5(a) indicates the Pauling's I_b for comparison. As seen in the figure, the general trend of I_P is consistent with I_b except certain vertical level shift and deviation for certain glasses. This feature implies that the electronic and ionic contributions as indicated by the present parameter I_P cannot be represented fully by the electronegativity difference of the material. Additionally, Fig. 5(b) shows the overview of I_P behavior in the $n\alpha$-ω_p/ω_0-I_P space, in which I_P exhibits monotonous variation and a diverging behavior as seen for the a parameter (Fig. 2(f)) is eliminated.

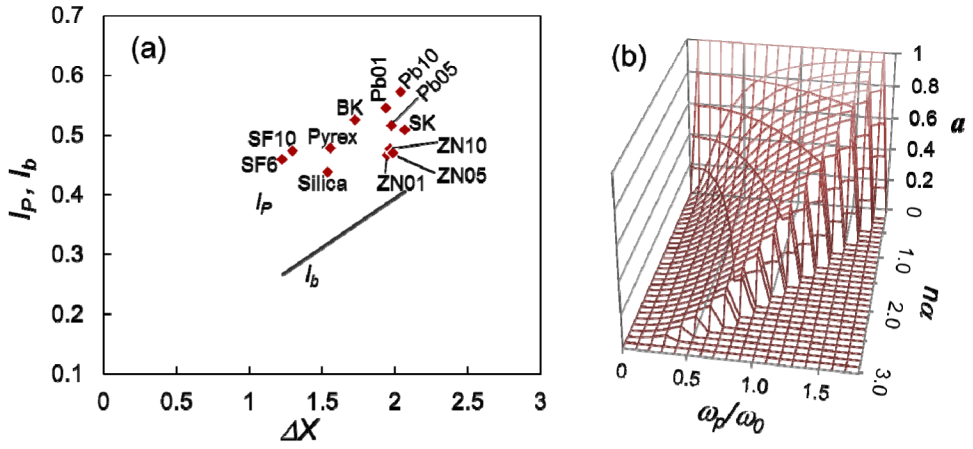

Fig. 5. (a) Relationship of measured values of polarization ionicity (I_p) as a function of electronegativity difference ΔX for silicate oxide glasses. A straight line indicates calculated line of Pauling's bond ionicity I_b. (b) Three dimensional view of the behavior of the ionicity contribution (I_P) to low-frequency dielectric constant in the plane of $n\alpha$ and ω_p/ω_0.

Table 3. Summary of values of the total microscopic susceptibility R^2, polarization ionicity I_P, electronegativity difference ΔX, and bond ionicity I_b determined for all glasses examined.

Glass	R^2	I_p	ΔX	I_b
ZNbKLSN01	2.421	0.465	1.95	0.386
ZNbKLSN05	2.426	0.476	1.97	0.386
ZNbKLSN10	2.413	0.468	1.99	0.392
PbNKLSN01	2.159	0.544	1.94	0.384
PbNKLSN05	2.199	0.515	1.98	0.390
PbNKLSN10	2.164	0.572	2.04	0.400
Silica	1.459	0.437	1.54	0.320
Pyrex	1.601	0.477	1.56	0.323
BK7	1.916	0.524	1.73	0.351
SK10	2.140	0.508	2.07	0.404
SF10	2.269	0.472	1.3	0.277
SF6	2.387	0.458	1.23	0.265

Optical Materials EXPRESS

Although the precise interrelation with material's physical and chemical properties is subject to further study, the presently defined polarization ionicity I_P is considered to be useful for characterizing the ionic contribution in the low-frequency dielectric constant of materials.

5. Dynamic response characteristics of the dielectric constant

We have seen so far that the dielectric constant properties of various multi-component glasses can be characterized by the single oscillator model taking account of the polarization ionicity. In the following, the dynamic property of the oscillator is compared among different glass materials so that the correlation between the dielectric constant and physical property of material is analyzed. For doing this, it is crucial to grasp the property of the basic network former SiO_2 common to all silicate oxide glasses. We have collected sub-THz range refractive index data on fused silica from other sources as shown in Table 4 [39–44] and analyzed their dynamic properties. For the optical dielectric constant values, the same value (2.13) as measured in [15] has been assumed for all fused silica data. The method for determining the characteristic frequency is the same as used in our previous work [21]. The dielectric function of Eq. (14) is expressed as a function of wavelength in the following form:

$$\frac{1}{\varepsilon - \varepsilon_\infty} = \left(\frac{2\pi c}{\omega_p^*}\right)^2 \left(\frac{1}{\lambda_0^2} - \frac{1}{\lambda^2}\right), \tag{21}$$

where λ_0 is the oscillator resonance wavelength and is correlated with ω_T by $\omega_T = 2\pi c/\lambda_0$. In Eq. (21), the damping term is neglected since the frequency range of our interest is much lower than the resonance. A plot of $1/(\varepsilon - \varepsilon_\infty)$ as a function of $1/\lambda^2$ gives a straight line, and its slope gives the value of ${\omega_p}^{*2}$ through ${\omega_p}^{*2} = (2\pi c)^2/[\text{slope}]$. Also the y-intercept for $1/\lambda^2 = 0$ ($\omega = 0$) is $1/(\varepsilon_s - \varepsilon_\infty)$, so [slope]/[y-intercept] yields ${\lambda_0}^2$ and hence ${\omega_T}^2$. Figure 6(a) and (b) show the plots of $1/(\varepsilon_s - \varepsilon_\infty)$ as functions of $1/\lambda^2$ for six groups' data on fused silica samples. The parameter values thus determined are summarized in Table 4.

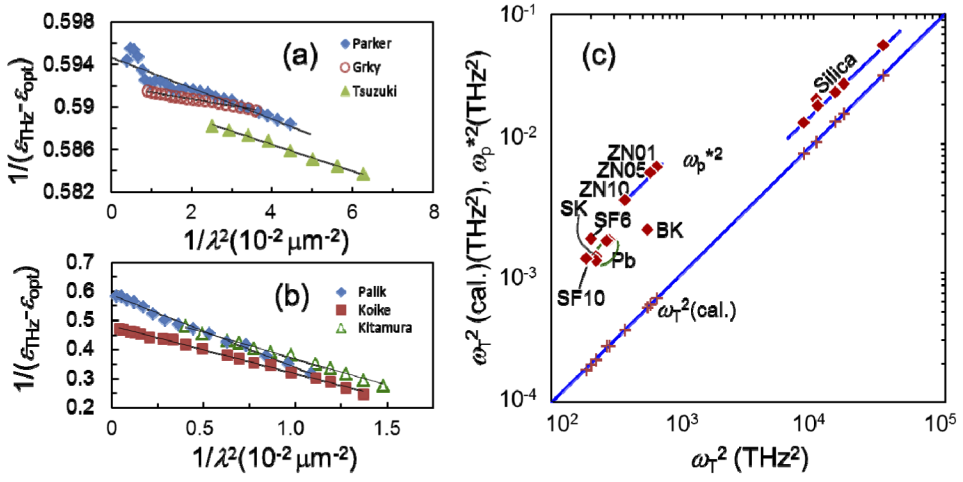

Fig. 6. (a) and (b) $1/[\varepsilon_s - \varepsilon_\infty]$ versus $1/\lambda^2$ plots for fused silica glasses taken from literature [39–41]. (c) Plots of calculated value of ${\omega_T}^2$ and measured value of ${\omega_p}^{*2}$ as functions of measured value of ${\omega_T}^2$ for silica and multi-component silicate oxide glasses.

Figure 6(c) shows the relationship of the experimentally determined value of ${\omega_T}^2$ versus the value calculated from the measured values of ε_s and ε_∞ by using Eqs. (12) and (13). This

Optical Materials EXPRESS

Table 4. Summary of THz and optical parameters determined for fused silica materials.

Group	ε_{THz}	ε_{opt}	$\omega_T{}^2$ (x10^4 THz^2)	${\omega_p}^{*2}/\omega_T{}^2$	$n\alpha$	ω_p/ω_0	ω_T/ω_0	Ref
Grischkovsky	3.82	2.13	3.36	1.69	0.819	0.797	0.842	[39]
Parker	3.81	2.13	1.46	1.68	0.819	0.796	0.842	[40]
Tsuzuki	3.83	2.13	1.69	1.69	0.819	0.798	0.842	[41]
Palik	3.84	2.13	0.838	1.71	0.819	0.800	0.840	[42]
Koike	4.24	2.13	1.05	2.08	0.819	0.860	0.812	[43]
Kitamura	4.24	2.13	1.07	1.82	0.819	0.860	0.813	[44]

indicates a nearly perfect agreement between them, confirming the relevance of the present single oscillator model for comparative analyses for different multi-component glasses. Figure 6(c) also shows the relationships between ${\omega_p}^{*2}$ and $\omega_T{}^2$ for all the silicate oxide glasses examined. Considering their mutual relationship as shown by Eq. (12), the vertical shift of each plot from the guide line for ${\omega_p}^{*2}=\omega_T{}^2$ indicates the quantity of (ε_s -ε_∞), which represents the difference in the amplitude of the oscillator in each glass material. There are appreciable differences in ${\omega_p}^{*2}$ and $\omega_T{}^2$ for different measurements on silica, and this is presumed to be due to the difference of physical and/or chemical nature of the specimen used, although exact detail of materials have not been given in cited publications. Appreciable changes of the polarizability and refractive index in infrared [45] and visible to ultraviolet [46] frequency regions have been reported for SiO_2 polymorphs. It is noted, however, that all the plots of ${\omega_p}^{*2}$ for different measurements come onto a straight line exhibiting a vertical distance within the range of ε_s -ε_∞=1.90+/-0.22 above the ${\omega_p}^{*2}=\omega_T{}^2$ line. This vertical shift of ${\omega_p}^{*2}$ from $\omega_T{}^2$ (=${\omega_p}^{*2}/\omega_T{}^2$) is relevant to other glasses: all vertical distances for other glasses agree, respectively, with the differences of ε_s -ε_∞, as can be verified in Table 2, which again confirms the consistency with the present single oscillator model. In the case of dielectric constants in optical region for other oxide glasses [47,48], a smooth (e.g. linear) trend is obtained between the oscillator strength (corresponding to ${\omega_p}^{*2}$) and resonance wavelength (corresponding to $1/\omega_T$). The present result is quite different from those primarily due to the ionicity effects emerging in the sub-THz domain.

Having acquired oscillator amplitude factors ${\omega_p}^{*2}$ for all glasses as shown in Fig. 6(c), it would be of interest to use them for analyzing parameters specific to material's physical/chemical properties. For an example, we take up the effective charge q^* of ion pair for evaluation. By using Eqs. (13) and (18) together with the definition, $\omega_0{}^2=D/\mu$, the following relation is readily derived:

$$q^* = \left(\frac{\varepsilon_0 V_m D}{N_A} \frac{9(\varepsilon_s - \varepsilon_\infty)}{(\varepsilon_s + 2)(\varepsilon_\infty + 2)} \right)^{1/2}. \tag{22}$$

The effective charge for the oxygen stretching motion (neglecting non-central motions) in silica glass is determined by using the central force constant of 600 N/m [49,50] to be 3.91×10^{-19} C (q*/e=2.45), which is consistent with the values reported in literature [50,51]. Since the value of D is not known precisely for all the glasses examined, we assume here a constant D as a first order approximation. This assumption would not be inconsistent with the slow variation of the optical dielectric constant (much suppressed than for $\omega_T{}^2$) for most of multi-component glasses. The obtained relationship of q^* normalized by the value for silica glass as a function of the total microscopic susceptibility R^2 is shown in Fig. 7. This result suggests the increase of the effective charge in multi-component glasses as R^2 increases. If D were assumed to gradually decrease for increasing R^2 (for instance to compensate the V_m variation), the slope of q^* increase for R^2 would become less pronounced.

Although the values of q^* as determined by Eq. (22) may not be conclusive due to the present simplified assumptions, qualitative trend of the effective charge increase has been found for those

Optical Materials EXPRESS

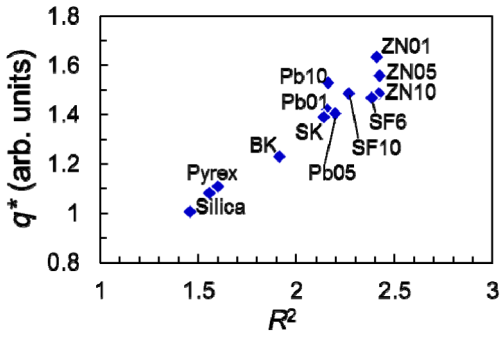

Fig. 7. Relationship of q^* normalized by the value for silica glass as a function of R^2 for multi-component silicate oxide glasses. The value of q^* has been determined by assuming a constant force constant D for all glasses.

multi-component glasses. Considering that the ion core displacement induced dipole moment ($\omega_p{}^2/\omega_0{}^2$ in Eq. (8)) is rather small (refer to Table 2) and the large enhancement of the dielectric constant is attributed substantially to the effects of valence electrons in the surrounding electron cloud, the effective charge q^* of ion pair is supposed to be dominated by the electron configuration in the ions. In this regard, the change in the number of non-bridging oxygens and/or coordination structure associated with the structural differences among the glasses would have strong influence. In ZNbKLSNd glasses, Nb-O bonds of Nb_2O_5 penetrate into the SiO_4 tetrahedral based Si-O-Si network to leave nonbridging oxygens to enhance O^{2-} polarizability [52]. In SiO_2–PbO based system (SF10 and SF6), it has been reported that as the PbO concentration increases (> 40 mol%) PbO begins to play a network former role by forming high coordination number structures such as PbO_3 trigonal pyramid or PbO_4 square pyramid structures, leading to the creation of nonbridging oxygens and the increase of polarizability [53,54]. To interpret the enhancement of THz dielectric constant in large R^2 region, the effect of increase in μ (refer to Eq. (13)) due to the inclusion of heavier metal cations such as Pb (in SF and PbNKLSNd glasses) and Nb (in ZNbKLSNd glasses), must be a primary cause as we have pointed out in [21]. More detailed discussion on the specific structural change is subject to further investigation.

6. Conclusion

We have extensively organized the single oscillator based dielectric model to characterize the THz dielectric constant properties of multi-component silicate oxide glass materials by incorporating the local field effects and material's ionicity. The present model has been confirmed to satisfactorily describe the THz dielectric properties over a wide variety of multi-component silicate oxide glasses. This has provided a simple, systematic characterization methodology, in which only the high- and low-frequency dielectric constants and the characteristic oscillator frequency data enable the determination of all basic physical parameters of the material's low frequency dielectric characteristics. The polarization ionicity has been introduced to distinguish the ionic and covalent contributions to the low-frequency dielectric properties. For all the examined multi-component glasses with close polarization ionicity values (0.48-0.55), a unique parameter (microscopic total susceptibility) has been demonstrated to be significant to systematically explain all the basic dielectric parameters. The polarization ionicity has also been shown to interpret the dielectric properties of multi-component glasses more precisely than the conventional bond ionicity. Correlation of the dynamic oscillator parameters (frequency and amplitude) have been demonstrated and used for arguing physical mechanism of the enhancement of low frequency dielectric constant. The highest THz dielectric constant (13.5-13.7) in ZNbKLSNd glasses

Optical Materials EXPRESS

has been ascribed to its physical feature including the smaller ion reduced mass and increased effective ionic charge in comparison with those in other multi-component silicate oxide glasses. The present characterization methodology would be useful for better understanding and design of THz dielectric properties of multi-component glasses and other non-crystalline insulating materials.

Funding. Ministry of Science and Technology, Taiwan (# MOST 106-2112-M-007-022-MY2, # MOST 110-2923-E-007-006).

Acknowledgments. Dr. Doddoji Ramachari is thankful to Ministry of Science and Technology, Taiwan for the award of Postdoctoral Fellowship. The authors thank Chao-Kai Wang and Chun-Ling Yen for taking the THz-TDS data of the samples reported in this work.

Disclosures. The authors declare no conflicts of interest.

References

1. X.-C. Zhang and J.-Z. Xu, *Introduction to THz Wave Photonics* (Springer, 2010).
2. T. Nagatsuma, G. Ducournau, and C. C. Renaud, "Advances in terahertz communications accelerated by photonics," Nat. Photonics **10**(6), 371–379 (2016).
3. P. U. Jepsen, D. G. Cooke, and M. Koch, "Terahertz spectroscopy and imaging – Modern techniques and applications," Laser Photonics Rev. **5**(1), 124–166 (2011).
4. M. Naftaly, N. Vieweg, and A. Deninger, "Industrial Applications of Terahertz Sensing: State of Play," Sensors **19**(19), 4203 (2019).
5. G. C. Righini, I. Cacciari, A. Tajani, and M. Brenci, "Terahertz flexible waveguides: an overview," Proc. SPIE **7366**, 73660Z (2009).
6. M. Zalkovskij, A. C. Strikwerda, K. Iwaszczuk, A. Popescu, D. Savastru, R. Malureanu, A. V. Lavrinenko, and P. U. Jepsen, "Terahertz-induced Kerr effect in amorphous chalcogenide glasses," Appl. Phys. Lett. **103**(22), 221102 (2013).
7. J. E. Shelby, *Introduction to Glass Science and Technology*, 2nd ed. (The Royal Society of Chemistry, 2005).
8. A. Jha, *Inorganic Glasses for Photonics: Fundamentals, Engineering and Applications* (John Wiley & Sons, 2016).
9. W. G. Spitzer, Robert C. Miller, D. A. Kleinman, and L. E. Howarth, "Far infrared dielectric dispersion in $BaTiO_3$, $SrTiO_3$, and TiO_2," Phys. Rev. **126**(5), 1710–1721 (1962).
10. U. Strom and P. C. Taylor, "Temperature and frefluency dependences of the far-infrared and microwave optical absorption in amorphous materials," Phys. Rev. B **16**(12), 5512–5522 (1977).
11. M. Herzberger and C. D. Salzberg, "Refractive indices of infrared optical materials and color correction of infrared lenses," J. Opt. Soc. Am. **52**(4), 420–427 (1962).
12. L. Ghivelder and W. A. Phillips, "Far infrared absorption in disordered solids," J. Non-Cryst. Solids **109**(2-3), 280–288 (1989).
13. S. Kojima, H. Kitahara, S. Nishizawa, Y. S. Yang, and M. Wada Takeda, "Terahertz time-domain spectroscopy of low-energy excitations in glasses," J. Mol. Struct. **744-747**, 243–246 (2005).
14. E. P. J. Parrott, J. A. Zeitler, G. Simon, B. Hehlen, L. F. Gladden, S. N. Taraskin, and S. R. Elliott, "Atomic charge distribution in sodosilicate glasses from terahertz time-domain spectroscopy," Phys. Rev. B **82**(14), 140203 (2010).
15. M. Naftaly and R. E. Miles, "Terahertz time-domain spectroscopy of silicate glasses and the relationship to material properties," J. Appl. Phys. **102**(4), 043517 (2007).
16. D. K. Dobesh, S. K. Sundaram, and R. E. Youngman, "Femtosecond laser pulse-induced structural modification of lanthanum aluminosilicate glasses: refractive indices in visible vs. terahertz frequency regions," J. Infrared, Millimeter, Terahertz Waves **41**(2), 171–193 (2020).
17. A. Ravagli, M. Naftaly, C. Craig, E. Weatherby, and D.W. Hewak, "Dielectric and structural characterisation of chalcogenide glasses via terahertz time-domain spectroscopy," Opt. Mater. **69**, 339–343 (2017).
18. S. B. Kang, M. H. Kwak, B. J. Park, S. Kim, H-C. Ryu, D. C. Chung, S. Y. Jeong, D. W. Kang, S. K. Choi, M. C. Paek, E-J. Cha, and K. Y. Kang, "Optical and dielectric properties of chalcogenide glasses at terahertz frequencies," ETRI J. **31**(6), 667–674 (2009).
19. M. Zalkovskij, C. Z. Bisgaard, A. Novitsky, R. Malureanu, and D. Savastru, "Ultrabroadband terahertz spectroscopy of chalcogenide glasses," Appl. Phys. Lett. **100**(3), 031901 (2012).
20. D. Ramachari, C.-S. Yang, O. Wada, T. Uchino, and C.-L. Pan, "High-refractive index, low-loss oxyfluorosilicate glasses for sub-THz and millimeter wave applications," J. Appl. Phys. **125**(15), 151609 (2019).
21. O. Wada, D. Ramachari, C.-S. Yang, T. Uchino, and C.-L. Pan, "High refractive index properties of oxyfluorosilicate glasses and a unified dielectric model of silicate oxide glasses in sub-terahertz frequency region," Opt. Mater. Express **10**(2), 607–621 (2020).
22. G. Burns, *Solid State Physics* (Academic Press, 1985).
23. G. Grosso and G. P. Parravicini, *Solid State Physics*, 2nd ed. (Elsevier, 2014)
24. V. Dimitrov and T. Komatsu, "Electronic polarizability, optical basicity and non-linear optical properties of oxide glasses," J. Non-Cryst. Solids **249**(2-3), 160–179 (1999).

Optical Materials EXPRESS

25. C. -S. Yang, C. -H. Chang, M. -H. Lin, P. -C. Yu, O. Wada, and C. -L. Pan, "THz conductivities of indium-tin-oxide nanowhiskers as a graded-refractive-index structure," Opt. Express **21**(14), 16670–16682 (2013)..
26. N. W. Ashcroft and N. D. Mermin, *Solid State Physics*, Chap. 27 (Cengate Learning Ltd., 1976)
27. S. Wang, *Solid State Electronics*, Chap. 7 (McGraw-Hill, 1966).
28. P. Grosse, *FreieElektronen in Festkoerpern* (Springer-Verlag, 1979); Japanese translation by A. Kinbara and M. Mizuhashi, "*Dennshibussei no kiso*" (Ohmsha, 1993).
29. J. C. Phillips, "Ionicity of the chemical bond in crystals," Rev. Mod. Phys. **42**(3), 317–356 (1970).
30. G. Lucovsky, "Transition from thermally grown gate dielectrics to deposited gate dielectrics for advanced silicon devices: A classification scheme based on bond ionicity," J. Vac. Sci. Technol., A **19**(4), 1553–1561 (2001).
31. J. A. Duffy, "Ionic-covalent character of metal and nonmetal oxides," J. Phys. Chem. A **110**(49), 13245–13248 (2006).
32. L. Pauling, *The Nature of the Chemical Bond*, 3rd ed. (Cornell University, 1948)
33. W. A. Harrison, *Electronic Structures and the Properties of Solids: The Physics of the Chemical Bond* (W. H. Freeman, 1980).
34. J. A. Duffy, "Chemical Bonding in the Oxides of the Elements: A New Appraisal," J. Solid State Chem. **62**(2), 145–157 (1986).
35. R. R. Reddy, K. R. Gopal, K. Narasimhulu, L. S. S. Reddy, K. R. Kumar, C.V. K. Reddy, and S. N. Ahmed, "Correlation between optical electronegativity and refractive index of ternary chalcopyrites, semiconductors, insulators, oxides and alkali halides," Opt. Mater. **31**(2), 209–212 (2008).
36. Y. Guo, C.K. Kuo, and P. S. Nicholson, "The ionicity of binary oxides and silicates," Solid State Ionics **123**(1-4), 225–231 (1999).
37. A. R. West, *Basic Solid State Chemistry* (John Wiley, 1988).
38. P. Atkins, T. Overton, J. Rourke, M. Weller, and F. Armstrong, *Inorganic Chemistry*, 4th ed. (Oxford University Press, 2006)
39. D. Grischkowsky, S. Keiding, M. van Exter, and C. Fattinger, "Far-infrared time-domain spectroscopy with terahertz beams of dielectrics and semiconductors," J. Opt. Soc. Am. B **7**(10), 2006–2015 (1990).
40. T. J. Parker, J. E. Ford, and W. G. Chambers, "The Optical Constants of Pure Fused Quartz in the Far-Infrared," Infrared Phys. **18**(3), 215–219 (1978).
41. S. Tsuzuki, N. Kuzuu, H. Horikoshi, K. Saito, K. Yamamoto, and M. Tani, "Influence of OH-group concentration on optical properties of silica glass in terahertz frequency region," Appl. Phys. Express **8**(7), 072402 (2015).
42. E. D. Palik, ed. *Handbook of Optical Constants of Solids* (Academic Press, 1985).
43. C. Koike, H. Hasegawa, N. Asada, and T. Komatuzaki, "Optical constants of fíne particles for the infrared region," Mon. Not. Royal Astronomical. Soc. **239**(1), 127–137 (1989).
44. R. Kitamura, L. Pilon, and M. Jonasz, "Optical constants of silica glass from extreme ultraviolet to far infrared at near room temperature," Appl. Opt. **46**(33), 8118–8133 (2007).
45. R. A. B. Devine and T. Busani, "Molecular volume dependence of the electronic and ionic polarizabilities in TiO_2 and SiO_2," Appl. Phys. Lett. **86**(6), 062902 (2005).
46. O. L. Anderson and E. Shreiber, "The relation between refractive index and density of minerals related to the earth's mantle," J. Geophys. Res. **70**(6), 1463–1471 (1965).
47. S. Hirota and T. Izumitani, "Effects of cations on the inherent absorption wavelength and the oscillator strength of ultraviolet absorptions in borate glasses," J. Non-Cryst. Solids **29**(1), 109–117 (1978).
48. K. Yoshimoto, A. Masuno, M. Ueda, H. Inoue, H. Yamamoto, and T. Kawashima, "Low phonon energies and wideband optical windows of La_2O_3-Ga_2O_3 glasses prepared using an aerodynamic levitation technique," Sci. Rep. **7**(1), 45600 (2017).
49. R. A. B. Devine, "Ion implantation- and radiation-induced structural modifications in amorphous SiO_2," J. Non-Cryst. Solids **152**(1), 50–58 (1993).
50. I. P. Lisovskii, V. G. Litovchenko, V. G. Lozinskii, and G. I. Steblovskii, "IR spectroscopic investigation of SiO_2 film structure," Thin Solid Films **213**(2), 164–169 (1992).
51. A. Lehmann, L. Schumann, and H. Hubner, "Optical phonons in amorphous silicon oxides I. Calculation of the density of states and interpretation of LO-TO splitting of amorphous SiO_2," phys. stat. sol. (b) **117**(2), 689–698 (1983).
52. R. S. Chaliha, K. Annapurna, A. Tarafder, V. S. Tiwari, P. K. Gupta, and B. Karmakar, "Luminescence and dielectric properties of nano-structured Eu^{3+}:K_2O–Nb_2O_5–SiO_2 glass-ceramics," Solid State Sci. **11**(8), 1325–1332 (2009).
53. V. V. Dimitrov, S. -N. Kim, T. Yoko, and S. Sakka, "Third harmonic generation in PbO-SiO_2 and PbO-B_2O_3 glasses," J. Ceram. Soc. Jpn. **101**(1169), 59–63 (1993).
54. P. W. Wang and L. Zhang, "Structural role of lead in lead silicate glasses derived from XPS spectra," J. Non-Cryst. Solids **194**(1-2), 129–134 (1996).